JACS
JOURNAL OF THE AMERICAN CHEMICAL SOCIETY

ARTICLE

pubs.acs.org/JACS

Transparent Conductors from Carbon Nanotubes LBL-Assembled with Polymer Dopant with $\pi-\pi$ Electron Transfer

Jian Zhu,[†] Bong Sup Shim,[†,∥] Matthew Di Prima,[†] and Nicholas A. Kotov*[,†,‡,§]

[†]Department of Chemical Engineering, [‡]Department of Materials Science and Engineering, and [§]Department of Biomedical Engineering, University of Michigan, Ann Arbor, Michigan 48109, United States

Supporting Information

ABSTRACT: Single-walled carbon nanotube (SWNT) and other carbon-based coatings are being considered as replacements for indium tin oxide (ITO). The problems of transparent conductors (TCs) coatings from SWNT and similar materials include poor mechanical properties, high roughness, low temperature resilience, and fast loss of conductivity. The simultaneous realization of these desirable characteristics can be achieved using high structural control of layer-by-layer (LBL) deposition, which is demonstrated by the assembly of hydroethyl cellulose (HOCS) and sulfonated polyetheretherketone (SPEEK)-SWNTs. A new type of SWNT doping based on electron transfer from valence bands of nanotubes to unoccupied levels of SPEEK through $\pi-\pi$ interactions was identified for this system. It leads to a conductivity of 1.1×10^5 S/m at 66 wt % loadings of SWNT. This is better than other polymer/SWNT composites and translates into surface conductivity of 920 Ω/□ and transmittance of 86.7% at 550 nm. The prepared LBL films also revealed unusually high temperature resilience up to 500 °C, and low roughness of 3.5 nm (ITO glass −2.4 nm). Tensile modulus, ultimate strength, and toughness of such coatings are 13 ± 2 GPa, 366 ± 35 MPa, and 8 ± 3 kJ/m^3, respectively, and exceed corresponding parameters of all similar TCs. The cumulative figure of merit, $\prod_{TC}$, which included the critical failure strain relevant for flexible electronics, was $\prod_{TC} = 0.022$ and should be compared to $\prod_{TC} = 0.006$ for commercial ITO. Further optimization is possible using stratified nanoscale coatings and improved doping from the macromolecular LBL components.

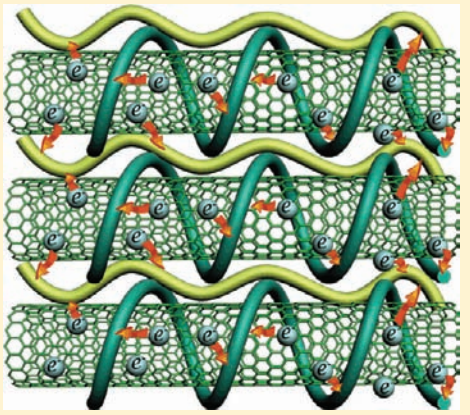

INTRODUCTION

Simultaneous optimization of several critical properties at the same time is one of the most fundamental challenges of materials science. Quite often the properties appear to be orthogonal, making this task very difficult and often haphazard. Examples of orthogonal properties and the difficulties of combining them can be encountered in virtually any area of both advanced and traditional materials. To give examples of such difficulties, one can look into the development of materials for neuroprosthetic devices, which require long-term biocompatibility, electrical conductivity, and flexibility,[1] materials for batteries and fuel cells, which require high ionic conductivity, high sheer modulus, and high temperature resilience,[2−4] or materials for aviation, which require high toughness, high electrical conductivity, and low density. Transparent conductors (TCs) can also be one of the best examples of materials with inherently orthogonal properties requiring high transparency and conductivity at the same time. Moreover, they also represent one of the most significant needs for several current technologies, drawing much attention to these materials.[5−10]

The most common TC is indium tin oxide (ITO), which is ubiquitous for information processing devices including the laptop computer on which this sentence was typed. ITO suffers from brittleness and scarcity of raw materials.[7,8,10−13] Ever increasing use of electronics, the need for flexible and potentially wearable devices, and new energy conversion technologies bring additional challenges for TCs. Considering different coatings as ITO replacements, they need to be comparable in conductivity and transparency to ITO, mechanically robust, thermally and environmentally stable, compatible with other processing stages, and easily available. Such multiparameter optimization requires the development of new chemical approaches to structural tuning of potential TC candidates.

No optimum material has been found so far to replace ITO and completely satisfy the technological demands of, for instance, flexible electronics. Amorphous metal oxide semiconductors, such as the In−Ga−Zn−O system, were developed to deposit on polymer substrate at low temperature, but their conductivity and mechanical flexibility are very limited.[14] Metal gratings and nanowire meshes have been demonstrated as one of the possible solutions, which can be particularly useful for EMI shielding and some display applications.[12,15−17] However, the approach suffers from formidable cost of complex nanoimprint technologies,[15,17] scale-up difficulties, and problems associated with light absorbance and scattering of nanowire

Received: January 11, 2011
Published: April 27, 2011

dx.doi.org/10.1021/ja111687t | J. Am. Chem. Soc. 2011, 133, 7450–7460

materials.[16] In addition, the properties of thin coatings have limited reproducibility.[12]

Electroactive polymers, such as polythiophenes,[18,19] have also been examined as potential TCs; however, these materials are usually rather resistive and display intense coloration. Some of the more encouraging candidates are thin film from single-walled carbon nanotubes (SWNTs) and graphene sheets.[20] Although absorptive in the visible range, individual SWNTs and graphene sheets have exceptional conductivity and mechanical properties, allowing them to be good candidates for low surface resistance and high strength TCs.

A nearly ideal SWNT- or graphene-based TC should have a sheet resistance of <50 Ω/□ at 85% transparency,[10] or 100 Ω/□ at 90%.[8] Considering strong absorption of carbon-based materials in visible range of spectrum, the bulk conductivity of the coatings should be at least 5.3×10^5 S/m to meet these requirements.[8] Current state-of-the-art SWNT TCs have a sheet resistance of ca. 300 Ω/□ at 90% transmittance and 100 Ω/□ at 80% transmittance with some variations depending on the methods used.[7−10] The conductivities of these coatings range from 1.6×10^5 to 2×10^5 S/m,[7,8] that is, 2−3 times below the needed performance. Graphene (G) and chemically similar material often identified as reduced graphene oxide (rGO) generated a lot of excitement in the TCs field. However, one also needs to admit that they often performed much worse than SWNT TCs with some G/rGO thin films having 1000 Ω/□ at 70% transparency.[21] Materials from G and rGO typically showed conductivities below 5.5×10^4 S/m.[22] The pathway to improve TC performance was suggested to be via strong doping with electron acceptors, but such doping detrimentally affects temperature resilience and compatibility with other electronic components.[23] Nevertheless, for G-based TCs, surface resistance can be reduced further to 30 Ω/□ at 90% transparency when high-quality G sheets are produced by chemical vapor deposition (CVD) method combined with high doping.[24]

Despite the impressive efforts, the current SWNT and G-based TCs share several still-to-be-solved challenges:

(1) Small molecules, such as acid,[25] $SOCl_2$,[26] and $AuCl_3$,[27] are often used to improve the conductivity through doping and reducing contact resistances between SWNTs or G.[24,28] However, these dopants are mobile and known to spontaneously escape from the carbon-based matrices, thus resulting in the inevitable deterioration of electrical properties.[23,28] Many electron acceptor (Lewis acid) dopants are becoming reduced or lost at even slightly elevated or even room temperatures by SWNTs, G, or rGO.[23] Additionally, the chemicals used for doping are corrosive; they can destroy contacts in electronic devices and poison surrounding materials, such as emissive layers in OLEDs.[8] Some nonvolatile organic polymers can also induce doping.[29] However, up to now they were difficult to use and often caused high contact resistance between SWNTs[29] or were relatively weak dopants aiming to reduce Schottky barriers in SWNT transistors.[30]

(2) Uniformity of conductive pathways throughout the material and low surface roughness are needed to make efficient and long-living electronic devices.[8−10] Rough, porous, and nonuniform conductive networks of many SWNT and G/rGO polymer composites result in low conductivity. Traditional techniques in this area yielded, so far, composites with bulk conductivities only ca. 10 S/m.[8] SWNT- and G-based coating without polymers gives much more conductive coatings, but adhesion to glass/plastic substrates and flexural robustness suffer. Smooth, virtually nonporous, and uniform coatings for SWNT or G/rGO composite with polymer or otherwise are preferred from the perspective of device longevity as well.

(3) Mechanical properties of SWNT- and G/rGO-based coatings are often insufficient for the long-term use under bending, stretching, and other stresses. Moreover, they are being studied much less than electrical properties,[8,31] which could be attributed to the more traditional view of TCs as coatings for flat solid substrates, such as glass. TCs improving ITO performance on bendable and stretchable substrates, for instance plastics, are much needed. Much better understanding of the fundamental relations between stress and strain on one side, transparency and conductivity on the other side, has to be established.

These challenges, which must be addressed simultaneously, make it difficult to utilize the classical techniques for synthesis of composite materials and coatings. It is much easier to address one property at a time to gradually approach the optimal combination. Yet quite often it is discovered along the way that some of these properties are difficult to combine together. For instance, addition of some polymers makes possible the improvement of mechanical properties but drastically reduces the conductivity and thermal stability of TCs. In a nearly ideal case, a minimal amount of mechanically robust polymer should bind SWNTs to themselves and to the substrate while providing charge carrier doping. The dual function of the polymer limits the choice of processing/synthetic techniques and underscores the importance of the nanometer-scale control of the structure in the resulting coatings. Layer-by-layer (LBL) assembly is likely to be one of a few techniques that make possible fine control over materials structure and much simpler combination of multiple properties,[32−34] including those important for TCs.[35] Easy-to-make conformal coatings with meticulously controlled thickness are characteristic for LBL. Overall, LBL represents a method that is difficult to pass by when considering the fabrication of TC materials and the academic challenge of attaining multiple functional characteristics.

Therefore, this Article endeavors to seek for new solutions to TC challenges by taking advantage of LBL engineering method. As such, we designed LBL multilayers (Figure 1A), which employ sulfonated polyetheretherketone (SPEEK, Figure 1C) as a new stabilizer for SWNTs and hydroxyethyl cellulose (HOCS, Figure 1B) as a new molecule glue. It was demonstrated that they could serve simultaneously as dopants. Moreover, these polymers were derived from macromolecules with outstanding mechanical properties (Figure 1C),[36] which would influence positively on the robustness of TCs. Both polymers are permanently locked in the coating through intricate interdigitation.[32] This structural feature was expected to impart both uniformity of conductive networks and thermal resilience. The prepared $(HOCS/SPEEK−SWNT)_n$ composite coatings were found to have a conductivity of 1.1×10^5 S/m and ultimate strength of 360 ± 35 MPa. A sheet resistance of 920 Ω/□ with 86.7% transmittance was achieved. Although without record conductivity, we succeeded in complete elimination of mobile, volatile, and corrosive dopants. Moreover, a new approach to SWNT doping was identified in this study. Unlike strong Brønsted and Lewis acids, the doping is based on electron transfer from several valence bands of SWNTs to low lying unoccupied levels of

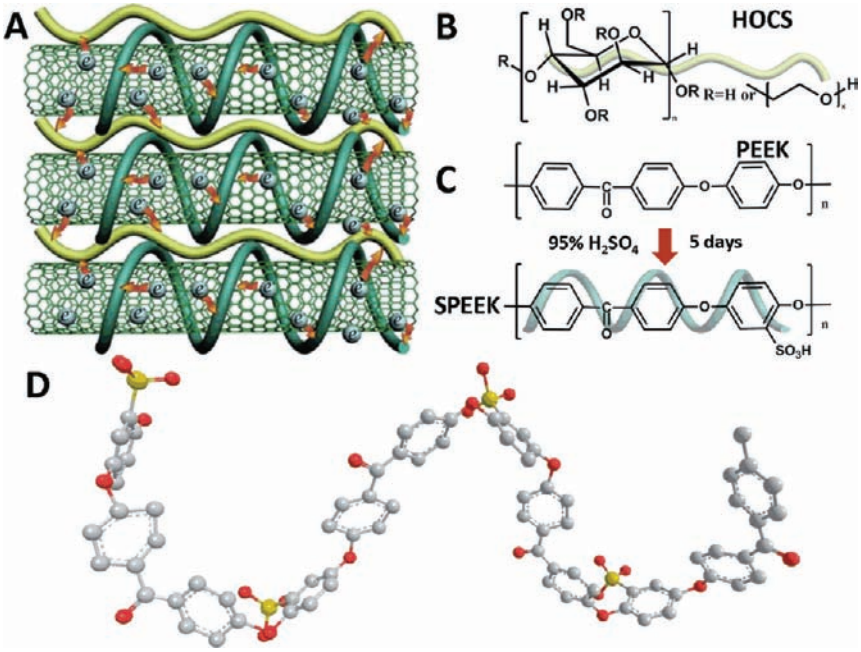

Figure 1. (A) Proposed ideal architecture for LBL films described in this Article. The red arrows indicate hole-doping from the surrounding polymers. SPEEK, green macromolecules; HOCS, yellow macromolecules. (B) Chemical structure of hydroxyethyl cellulose (HOCS) and (C) poly(etheretherketone) (PEEK). (C) Chemical structure of sulfonated PEEK (SPEEK). (D) Ball-and-stick model of SPEEK in the minimal energy state calculated by Molecular Mechanics (MM2) algorithm. Gray spheres are assigned to carbon atoms, red to oxygen atoms, and yellow to sulfur atoms. Hydrogen atoms are omitted for greater clarity.

SPEEK in the π-stacked electronic system. Because of substantially higher placement of the lowest unoccupied molecular orbital (LUMO) of other structurally related compounds, the doping was impossible or ineffective. Additionally, a cumulative electrical/optical/mechanical performance expressed as figure of merit, $\prod_{TC}$,[35] substantially exceeding that of ITO was achieved. We also observed that the produced TCs were thermally stable with little decomposition until 500 °C, which is quite remarkable for polymer coatings. The findings of this study can potentially be applied to other carbon-based TCs and serve as a convenient model to establish structure−property relations with multiple coordinates and optimization targets.

EXPERIMENTAL SECTION

Sulfonation of Poly(etheretherketone) (PEEK). Fine powders of PEEK450P were purchased from Victrex and were gradually dissolved in 95−98% sulfuric acid at a concentration of 2.5 g/100 mL. The mixture was stirred at room temperature for a period of 5 days. The sulfonated powders were then precipitated from solution with a 5-fold excess of deionized (DI) water at 0 °C and thoroughly washed with water until neutral pH. Subsequently, the product, that is, sulfonated PEEK (SPEEK), was dried at 50 °C under vacuum for 24 h. The stock powder of SPEEK can be easily dissolved in boiling water.

Preparation of SWNT Dispersions Stabilized with SPEEK. SWNTs were bought from Carbon Solutions Inc. and carried product designations as P2 or P3. P2 and P3 SWNTs have similar purity (>90%), but P3 carried a greater density of −COOH groups than did P2 (see descriptions at http://www.carbonsolution.com). 0.5 mg/mL of P2 or P3 SWNTs was dispersed by 2 and 1 mg/mL SPEEK in DI water, respectively. Homogenous dispersions were obtained by sonication for 12 h. The pH of the solution can be easily adjusted by NaOH.

Energy Optimization and Molecular Orbital Calculation of Polymer. MM2 force field modeling with default parameters was used to roughly calculate the relaxed state of polymer in software of ChemBio3D 2010 from CambridgeSoft Corporation. The energy of molecular orbitals was calculated by UV−vis spectra simulator (version 1.5.3) from NanoHub.org. The tool uses the SCF-MO package ORCA to calculate molecular electronic structures. Excited states can be calculated via CI-singles (CIS) with the semiempirical Hamiltonian ZINDO.

Layer-by-Layer Assembly. In a typical LBL cycle, glass or silicon slides cleaned by piranha solution for 24 h were immersed in 0.1 wt % HOCS for 1 min, rinsed in DI water, and then dried with compressed air. Subsequently, these slides were dipped into the SPEEK-stabilized SWNT solutions for 2 min, followed by similar rinsing and drying. The above cycle can be repeated n times to obtain desirable thickness. The resulting coating or free-standing film will be designated as $[HOCS/SPEEK−SWNT]_n$. The LBL film was generally assembled in pH 10 SWNT dispersions unless specifically noted. To deposit LBL film onto polymer substrate, such as PET, the substrate was immersed into 1% polyethylenimine for 1 min to make it hydrophilic, so then a deposition process similar to that on glass substrate can be followed. To ensure the good quality of films on PET, it is recommended to fix PET on glass to avoid bending during handling.

Characterization. UV−vis spectra throughout the study were obtained on a 8453 UV−vis ChemStation spectrophotometer (Agilent Technologies). The supernatants of SWNT dispersions after centrifugation at 10 000 rpm for 2 h were used to obtain the UV−vis spectra.

The degree of sulfonation of PEEK was evaluated by attenuated total reflection Fourier transform infrared spectroscopy (ATR-FTIR) and X-ray photoelectron spectroscopy (XPS). ATR-FTIR spectroscopy was performed on a Nicolet 6700 spectrometer utilizing the grazing angle accessory (Smart SAGA) at a grazing angle of 85°. All of the samples for IR were prepared by spin-coating of several drops of solutions onto gold-covered glass. PEEK was dissolved in methanesulphonic acid (MSA, Sigma-Aldrich), while SPEEK was dissolved in ethanol at room temperature. PEEK showed no trace of sulfonation even after 8 days in MSA.[37] Powder samples were examined by a Kratos AXIS Ultra Imaging X-ray photoelectron spectrometer. All spectra were calibrated with the

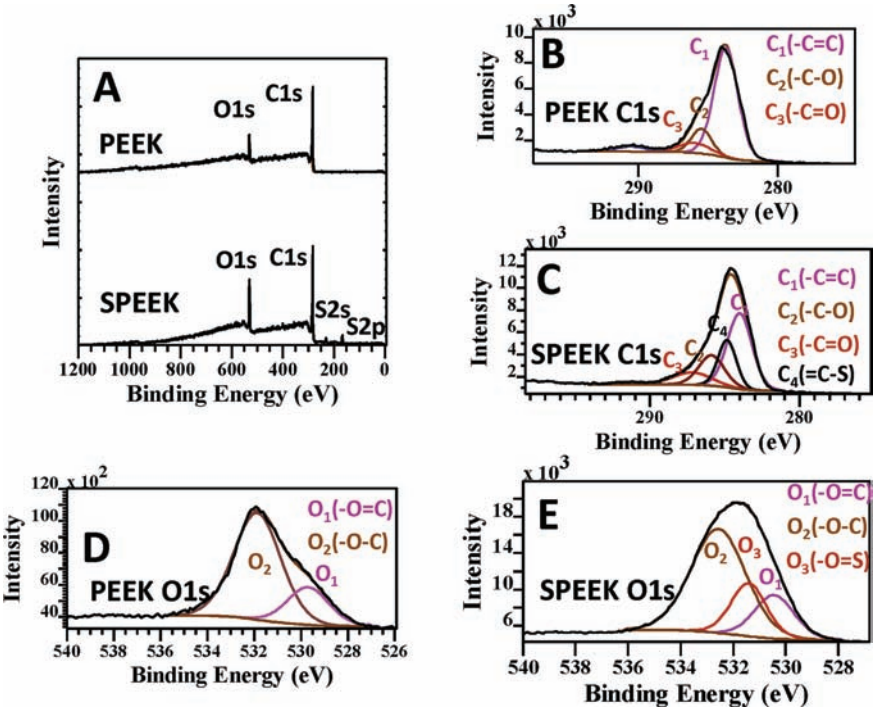

Figure 2. X-ray photoelectron spectroscopy (XPS) spectra of polyetheretherketone (PEEK) and sulfonated PEEK (SPEEK). (A) Wide scan survey spectrum. (B,C) C1s spectra of PEEK and SPEEK. (D,E) O1s spectra of PEEK and SPEEK.

C1s photoemission peak for sp^2 hybridized carbons at 284.7 eV to compensate for the effect of charging. Component fitting of the photoemission spectra was performed with mixed Gaussian/Lorentzian model after a Shirley-type background subtraction.

The transmittance of LBL films on glass substrate was measured by UV−vis spectroscopy with a clean glass slide as background. In a typical LBL process, both sides of the glass slide were coated with films. To get the transmittance for only one side, the other side had to be carefully removed with wet soft tissue. The transmittance values of double sided film (T_2) and only one sided film (T_1) are usually related by the formula $T_1 = T_2^{-0.5}$, which can be easily derived from Beer's law.

The thickness of films on silicon wafers was measured by a J. A. Woolham Co. VASE spectroscopic ellipsometer by fitting Cauchy model. Mass growth of films was investigated by a quartz crystal microbalance (QCM) 200 from Stanford Research Systems. 5 MHz quartz crystals were used in all of the studies.

Tapping mode atomic force microscopy (AFM) images were obtained using a NanoScope IIIa atomic force microscope (AFM) from Veeco Instruments (Santa Barbara, CA). AFM tips are from Mikro-Masch with tip radius smaller than 10 nm. Sheet resistance was measured for films deposited on glass substrates using a Lucas S-302-4 four-point probe station with the Agilent 3440A multimeter. A series of 3−4 measurements were taken on each film, and the measurements then were averaged to give the final reported value and errors. At least two different batches of films at the same experimental conditions were measured to ensure the repeatability of the data. Scanning electron microscopy (SEM) images were obtained with an FEI Nova Nanolab dual-beam FIB and scanning electron microscope, and energy dispersive X-ray spectroscopy (EDAX) was conducted in the SEM's EDAX mode. Perkin-Elmer Pyris 1 TGA was used for thermal gravimetric analysis. Resonance Raman spectra were taken with a Dimension-P1 Raman system (Lambda Solutions, Inc.) with 532 nm excitation. Stress−strain curves of free-standing films were analyzed by a mechanical tester 100Q from TestResources Inc. at a constant rate of 0.01 mm/s. The test samples were 1 mm wide and 4−6 mm long.

RESULTS AND DISCUSSION

Preparation of the Polymer Dopant, SPEEK. SPEEK is obtained by an electrophilic aromatic substitution reaction toward poly(etheretherketone) (PEEK) (Figure 1C) with concentrated sulfuric acid at room temperature.[38] PEEK was selected as a parent polymer for this project due to (1) well-known mechanical properties, (2) a large number of phenyl rings capable of $\pi-\pi$ stacking with chemically similar aromatic rings in graphene walls of SWNTs, and (3) transparency in the visible range of the electromagnetic spectrum. Chemical modification in PEEK can lead to adjustment of energy levels of the π-orbitals to effect efficient doping. As such, electron-withdrawing functional groups were introduced into PEEK to provide hole-doping of SWNTs. Incidentally, the same group(s) can also make PEEK easily soluble in polar solvents. Therefore, SPEEK with electronegative easy-to-ionize sulfonic acid groups ($-SO_3H$) was expected to be an effective dopant and stabilizer to debundle SWNTs into individual nanotubes. Subsequent studies indicated that, although the original premise was correct, the mechanism of doping turned out to be very different and interesting from both fundamental and practical points of views.

X-ray photoelectron spectroscopy (XPS) was performed to verify the identity of the SPEEK products (Figure 2). As expected, the 2p photoemission peaks from sulfur are clearly observed, indicating the sulfonation of PEEK macromolecules. The atomic concentration of sulfur can be calculated to be 4.46% and agrees well with the suggested unit formula of SPEEK in Figure 1C with theoretical sulfur content of 4.00%. The C1s XPS band of PEEK (Figure 2B) has three components corresponding to C_1 (−C═C), C_2 (−C−O), and C_3 (−C═O).[39] After successful sulfonation (Figure 2C), a new XPS component designated as C_4 appears between C_1 (−C═C), C_2 (−C−O) peaks and is attributed to −C−S groups. A new oxygen XPS peak appearing

dx.doi.org/10.1021/ja111687t |J. Am. Chem. Soc. 2011, 133, 7450–7460

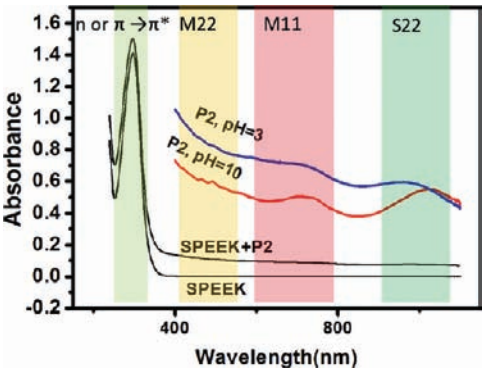

Figure 3. UV−vis spectroscopy of SPEEK aqueous solution and SPEEK-stabilized P2 SWNT dispersions under pH = 3 and pH = 10. The spectra at range of 400 nm and above were shown to highlight the difference between different pH's. The vertical colored bands indicate the spectral regions of electronic transitions contributing to the UV spectra. From left to right, lighter green, $\pi-\pi^*$ and $n-\pi^*$ transition in phenyl rings or C═O bond in SPEEK; yellow, M11 transition in SWNT; red, M22 transition in SWNT; green, S11 transition in SWNT.

between O_1 (−O═C) and O_2 (−O−C) components is indicative of O═S groups (O_3) (Figure 2D and E).[40]

The sulfonation of PEEK is also evident from FTIR spectra (Figure S1).[38] The 1657 cm^{-1} band is assigned to stretching vibrations of the carbonyl functional group, while 1599 and 1497 cm^{-1} are characteristic for stretching vibrations of aromatic rings; the 1228 cm^{-1} peak is typical for C−O stretching in the parent polymer. After sulfonation, the absorption band at 1497 cm^{-1} is replaced by two new peaks at 1432 and 1477 cm^{-1} characteristic of the phenyl rings vibration modes with $-SO_3H$ substitution. A new absorption band occurring at 1255, 1138, 1083, and 1025 cm^{-1} indicates the sulfonic acid groups in SPEEK.[38,41] The stretching vibration of S−O in the hydrosulfonate groups can be observed at the appropriate position at 1083 cm^{-1}.[41] To be noted, physical adsorption of sulfuric acid would not give changes in the phenyl ring characteristic region in FTIR and carbon emission peak in XPS.

SPEEK-Stabilized Dispersions of SWNTs. In the relaxed state of SPEEK through molecular mechanics calculations (Figure 1D), phenyl rings connected by carbonyl groups stay almost in-plane, while those connected by oxygen atoms tend to be perpendicular to each other. When interacting with SWNT, the flexible C−O−C bonds are expected to rotate and adjust to the shape of SWNT to maximize the overlap of π-orbitals between phenyl rings and graphene walls of SWNTs.[42,43] These molecular adjustments do not prevent the charged sulfonated groups in polymers from being accessible by water, thus facilitating the separation and stabilization of individual SWNTs through electrostatic repulsion.

In UV−vis spectra of SPEEK, the absorption near 300 nm in UV−vis spectra (Figure 3) can arise from both $\pi-\pi^*$ and $n-\pi^*$ transitions in phenyl rings or the C═O bond. In SPEEK-stabilized P2 SWNT dispersions, a slight increase in the absorbance of this band is observed. The van Hove nanotubes bands in the visible and NIR region (Figure 3) reveal interesting information about electronic interactions SPEEK and SWNT.[44−47] The bands[45] become sharper in basic dispersions as compared to the acidic conditions under the same preparation procedure, indicative of more exfoliated states of nanotubes due to increased ionization of SPEEK. One can also see a clear red shift in S22 (900−1100 nm) bands around 1100 nm when pH is changed from pH 3 to pH 10. Unlike many previous cases of acid

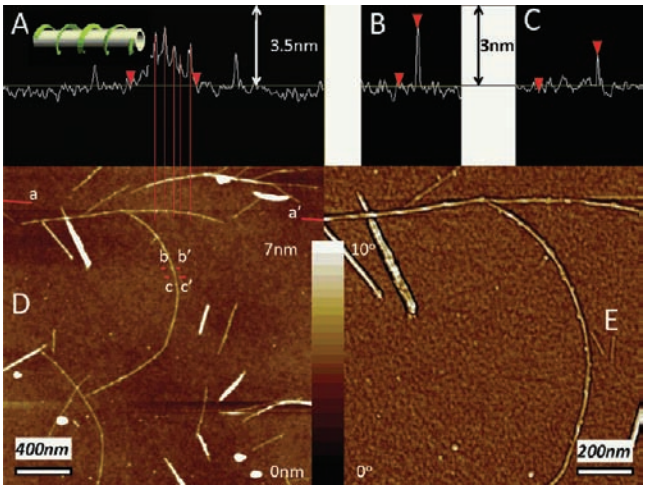

Figure 4. (A−C) Section analysis along a−a′, b−b′, and c−c′ lines in AFM height image (D). The a−a′ line goes along the axis of an individual SWNT wrapped with SPEEK, while b−b′ goes perpendicularly to the SPEEK-wrapped SWNT surface, and the c−c′ line is placed in the part where SWNT surface is bare. (E) A close-up phase image of nanotubes in (D). The cartoon in the inset of (A) demonstrates helical wrapping of SPEEK around SWNT.

doping,[35] this suggests the increased doping of SWNTs in basic conditions, which usually causes the bleaching and reappearance of S22 band at the longer wavelength.[27] This is attributed to the larger surface area of more dispersed SWNT, which facilitates more efficient charge transfer between SPEEK and nanotubes, while the presence of acid groups in this system has less or no significance on the doping process for the SPEEK−SWNT pair.

Atomic force microscopy (AFM) images of SWNT dispersion at pH 10 clearly display individual SWNTs with diameters around 1.4 ± 0.1 nm (Figure 4C), which agrees with their dimensions from the company specifications.[45] For macromolecules of interest for TC coatings, such as conductive polymers, both linear packing[48] and helical wrapping[43] were observed, dependent on the strength of interaction and rigidity of the polymeric chains.[49] In this system, one can see that SPEEK wraps SWNTs in a helical manner (Figure 4 D and E), indicating the ability of the polymeric chains to coil around the nanotubes. The tight contact between SPEEK and SWNTs indirectly confirms the strong attractive interactions between SPEEK and SWNTs. The pitch of the SPEEK helix on SWNTs is 62 nm (Figure 4A), which is similar to the pitch distance reported for DNA/SWNT hybrids.[50] At the same time, it is substantially longer than that for conductive polymer/SWNT hybrids with the pitch observed to be 14 nm.[43]

Unlike the continuous helixes shown for DNA/SWNT hybrids,[50] the periodicity of SPEEK/SWNT hybrids pitches is sometimes interrupted. The inconsistency of pitch distance arises from the relatively short chain of SPEEK,[50] estimated to be several hundred nanometers (for an average molecular weight of 50 kDa),[51] while the length of the studied DNAs molecules was ca. 1.4 μm.[50] Several molecular chains of SPEEK are needed to stabilize an individual SWNT, whose length is usually over 1 μm. The AFM analysis of cross sections along the Z-axis suggests that SPEEK "wrap" has a height of 2.2 ± 0.1 nm (Figure 4B). The thickness of polymer layer can thus be estimated to be (2.2−1.4)/2 = 0.4 nm,

which is consistent with a gap of 0.34 nm characteristic for a stack of two aromatic rings bonded by $\pi-\pi$ interaction.[52]

Layer-by-Layer Assembly. SPEEK-dispersed SWNTs were found to easily form multilayers with HOCS for both SWNT coatings and free-standing films. According to ellipsometry and quartz crystal microbalance (QCM) measurements (Figure 6B), the growth follows a linear fashion, with an average thickness of 3.7 ± 0.5 nm and mass deposition of 0.47 ± 0.08 $\mu g/cm^2$ for SWNT layers. Interestingly, the average thickness increment for HOCS layers is negative and is equal to −0.2 ± 0.4 nm, while mass increment is positive and equal to 0.10 ± 0.05 $\mu g/cm^2$. The overall density of the composite can be calculated to be 1.6 g/cm^3, which is close to the average density of constituent materials, and much greater than that of buckypaper prepared from filtration method[53] (Tables S1 and S2), which points to lower nanoscale porosity and excellent integration of polymers and nanotubes. The negative thickness increment with positive mass increment for each stage of HOCS adsorption stage is quite peculiar and indicates densification of the films. One can surmise that it occurs due to removal of a small amount of excessive SPEEK, which is not tightly wrapped around SWNTs. A control experiment shows that a layer of free SPEEK adsorbed on glass is indeed washed off by HOCS, being however unchanged after the DI water wash. Confirming the same point, LBL assembly of SPEEK (without SWNTs) and HOCS showed insignificant and erratic film growth pattern (Figure S2). One can also see here a manifestation of strong interaction between HOCS and SWNTs enabling the multilayer growth. These interactions are likely to include hydrophobic attraction and van der Waals forces between the sugar cycle and curved graphene sheet.[33,54] The presence of SWNTs in the LBL films also delocalizes negative charge on SPEEK due to their high polarizability[55,56] and axial anisotropy, which reduces localized electrostatic repulsion between adjacent SPEEK molecules that destabilizes the multilayers. This special assembly mechanism results in minimal incorporation of polymers in the coating while retaining highly accurate and predictable control over coating thickness. Because of the very thin polymer coatings, it is difficult to identify the layered structure in the composite even by TEM.[32]

The AFM image in Figure 5A shows that HOCS forms a smooth layer on the substrate. A dense and strictly in-plane orientation of SWNTs layer can be subsequently adsorbed onto HOCS (Figure 5C). In addition to SWNTs, some nanoscale particles also appear on the surface. Initially, these particles were believed to be amorphous carbon present in a small amount in SWNTs. However, a control experiment of direct adsorption of SPEEK onto HOCS also showed their presence (Figure 5B). Apparently, some of the molecular chains of SPEEK can be adsorbed onto the HOCS layers in a globular form. The number of SPEEK globules is reduced after depositing a layer of HOCS (Figure 5D). This is consistent with the negative thickness and positive mass increments observed in Figure 6B.

Optical and Electrical Properties. The transparency versus conductivity curves are dependent on multiple factors including the pH and type of the nanotubes. P2 dispersions give noticeably better overall transparency and sheet resistance (920 Ω/□ with 86.7%@550 nm) (Figure 6A) than does P3 due to lower degree of oxidation. The opto-electrical properties of LBL coatings at different pH for P2 or P3 are quite similar, except that the deposition was faster in the basic condition, especially for the type of P3. Higher pH usually gives better exfoliation of SWNT due to the more ionized state of sulfonic and carboxylic acid

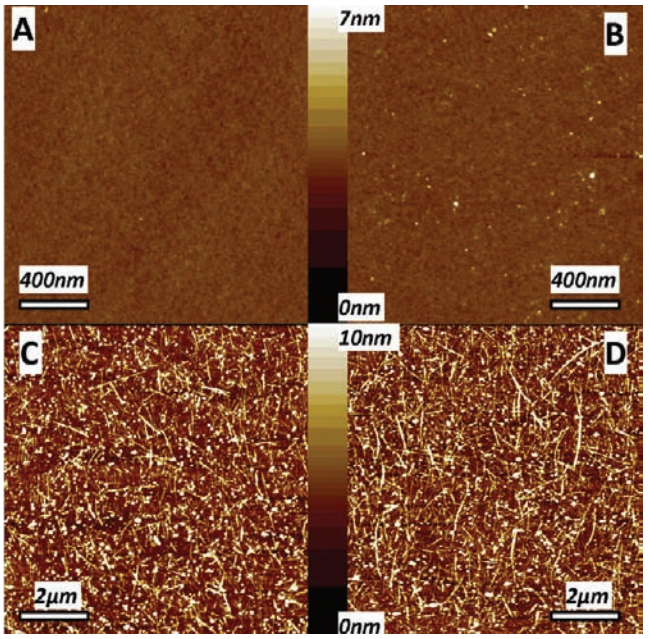

Figure 5. AFM height images of (A) HOCS layer on a silicon wafer, (B) $[HOCS/SPEEK]_1$without SWNT, (C) $[HOCS/SPEEK-P2]_1$ with SWNT on top, and (D) $[HOCS/SPEEK-P2]_{1.5}$ with HOCS on top.

group. The more dispersed state of SWNT can generate a higher concentration of individual SWNT to expedite adsorption. In addition, electrostatic attraction for the assembly can be stronger when more charged groups are on SWNTs.

To be noticed, the sheet resistance of SWNT coatings decreases when depositing an extra insulating layer of HOCS on top (Figure S3). This observation may contradict the conventional notion and multiple data[29,35] that addition of insulating matrix should decrease conductance, but is perfectly consistent with the mechanism of LBL deposition and expected changes in nanometer scale organization of the film. The improvement of conductivity results from the partial removal of SPEEK in HOCS solutions as discussed previously. Additionally, applying the HOCS layer could also result in densification of SWNT networks due to capillary effect and surface energy difference, thus lowering the conducting barriers and causing the unusual decrease in resistance. A similar effect was also recently observed after applying an insulating layer of tetraorthosilicate sol on top of SWNT networks, which is essential for passivation of SWNT coatings without sacrificing conductivity.[57] The densification of coatings can be indeed seen as the negative growth characteristic of HOCS layers (Figure 6B). As we can see later, addition of HOCS can also improve doping of SWNTs.

The conductivity of LBL assembled composites was evaluated by measuring the resistance and thickness of 200 bilayers to eliminate potential errors when working with thin hardly visible coatings. Robust free-standing films can be delaminated from glass substrate by HF (Figure 8A−C).[33,58] The thickness across 200 bilayer films denoted as $[HOCS/SPEEK-P2]_{200}$ was 1000 ± 40 nm, while $[HOCS/SPEEK-P3]_{200}$ was 620 ± 20 nm. The average thickness per bilayer can accordingly be calculated to be 5.0 ± 0.2 and 3.1 ± 0.1 nm, agreeable with ellipsometry measurements. The conductivity of $[HOCS/SPEEK-P2]_{200}$ is 1.1×10^5 S/m and turns lower when P3−SWNT are used, tha tis, 7.2×10^4 S/m. As a comparison, the P2 SWNT coatings made by different methods had conductivity ranging from 1.6×10^5 to 2×10^5 S/m,[7] while for P3 the conductivity was

dx.doi.org/10.1021/ja111687t |J. Am. Chem. Soc. 2011, 133, 7450–7460

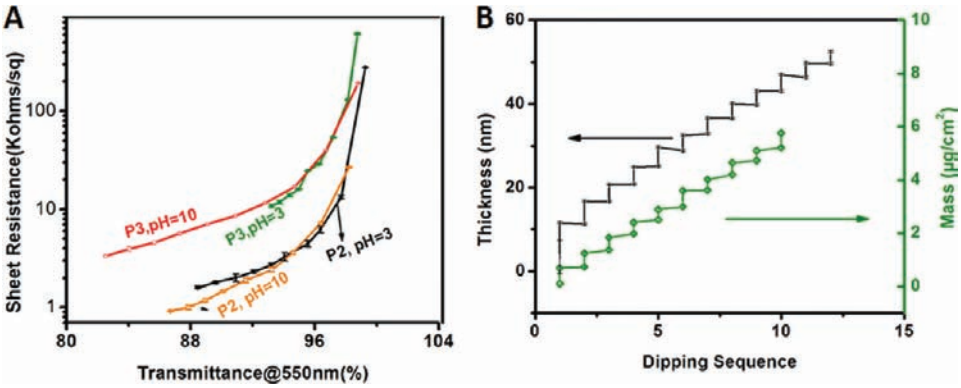

Figure 6. (A) Sheet resistance and transmittance@550 nm of P2 and P3 SWNT LBL thin films under different pH values. Ten LBL deposition cycles were made for each set of conditions. (B) Dependence of thickness and mass of $[HOCS/SPEEK-P2]_n$ assembled at pH 10 with the increasing number of LBL deposition cycles. A series of four measurements were taken on each film, and the measurements then were averaged to give the final reported value and errors. At least two different batches of films made at the same experimental conditions were measured to ensure the repeatability of the data. All of the measurements were performed on glass substrates.

7.3×10^4 S/m.[9] Unlike these coatings, which consist mostly of SWNTs, LBL assembled SWNT composites are quite remarkable in conductivity considering that they contained a lot of insulating matrix (34.38 wt % or 44.03 vol %, Supporting Information) and demonstrate both the capabilities of LBL in materials engineering and the importance of fine degree of structural control for these composites. The property is also superior to other SWNT/polymer composites made from other methods; for instance, SWNT/polystyrene composites with SWNT volume fraction as high as 50% were reported to have a conductivity of 1×10^4 S/m.[59] Even when the matrix was replaced by conductive polymers, conductivity only went up to 7×10^4 S/m.[60]

Mechanism of Doping. The transparency versus conductivity curve for $[HOCS/SPEEK-P2]_n$ indicates substantially higher conductivity for the same amount of deposited SWNT than for $[poly(vinyl\ alcohol)/poly(styrene\ sulfonate)-P2]_n$ or $[PVA/PSS-P2]_n$, which has a sheet resistance of 1790 Ω/□ with a transmittance of 85%@550 nm (Figure S4). This fact is indicative of possibly a different mechanism of doping than from $-SO_3H$ groups and prompted us to look into greater detail the electronic processes between SWNTs and SPEEK. The better overall performance of the studied film can be partially ascribed to the higher SWNT fraction obtained in the final film, which was estimated to be as high as 66 wt % (Supporting Information), as compared to 47 wt %[34] or 10 wt %[33] in previous studied SWNT LBL multilayer composites. However, this does not give a complete picture of the phenomenon. The in situ doping of SPEEK does play the key role here, which can be verified by Raman spectroscopy. The G band in the SWNT Raman spectrum undergoes a blue shift as a consequence of phonon stiffening induced by hole-doping.[27,29] The G band of LBL assembled SWNT film shows a clear blue-shift by about 10 cm^{-1} versus the original nanotubes (Figure 7A). Notably, this shift is comparable to that from such a strong dopant as $AuCl_3$[27] and is slightly larger than the shift from HNO_3 and H_2SO_4 doping,[29] which demonstrates that SWNTs in the film are indeed heavily doped. It is also known that the intensity of G′ band rises as the metallicity of the sample increases.[27,61] The effect of enhanced hole-doping is also manifested in the increased intensity of G′ band near 2675 cm^{-1} (Figure 7B). Similar shifts were also observed in P3 SWNT LBL films (Figure S6A).

The doping of SWNT in the LBL film can be contributed both by SPEEK and by HOCS, as can be shown by Raman spectra of their mixtures with SWNT (Figure 7A). A blue shift of 4 cm^{-1} for HOCS and of 6 cm^{-1} for SPEEK (pH = 10) was observed. The stronger shift (10 cm^{-1}) in the LBL film was a mutual and synergistic effect from both of the dopants. A much larger shift of 14 cm^{-1} occurred for SPEEK-P2 SWNT mixtures at pH = 3, which can be caused by residual traces of H_2SO_4 inside SPEEK. After being dried, the traces of H_2SO_4 can be locally concentrated to form even stronger dopant. However, there is no difference between the G band shifts in LBL-assembled films at different pH and even different thickness, which indicates that the impurities, such as H_2SO_4, are completely removed by the thorough rinsing in each of the LBL cycles and are not relevant for doping.

Independence of G band shift on pH and much greater conductivity observed for SPEEK than for PSS (Figure S6B) brings up the question about the chemical nature of the groups responsible for doping. The above observations are inconsistent with the mechanism based on hole-doping of SWNTs by $-SO_3H$ groups. Let us recall the fact that p-doping is the partial transfer of electrons from SWNTs to a dopant. For this reason, Brönsted and Lewis acids, such as concentrated H_2SO_4, HNO_3, or $AuCl_3$, are so effective when intercalated into SWNT bundles.[27,62] We also considered possibilities those other groups besides $-SO_3H$, for instance, $-SO_3^-$, $-C{=}O$, and multiple oxygen atoms in HOCS and SPEEK, could potentially act as local electron acceptors or donors (electron-doping). Yet none of these assumptions can consistently explain experimental data in this study. For example, $-SO_3^-$ group alone cannot cause a significant shift in the G band of SWNTs neither as a hole- or as an electron-dopant, based on the previous data for SWNT dispersions stabilized with sodium dodecyl sulfate.[63]

It is thus suggested that that the charge transfer process is mediated by the phenyl rings of SPEEK rather than the direct doping from $-SO_3H$ functional groups. To evaluate the possibility of this mechanism, molecule orbital calculations were performed to establish the relative energies of HOMO and LUMO orbitals in SPEEK. For comparative purposes, the same calculations were also performed for structurally related PSS (Figure S7A and C). The corresponding energy densities of state were also calculated[27] for a semiconducting SWNT (19, 0) with

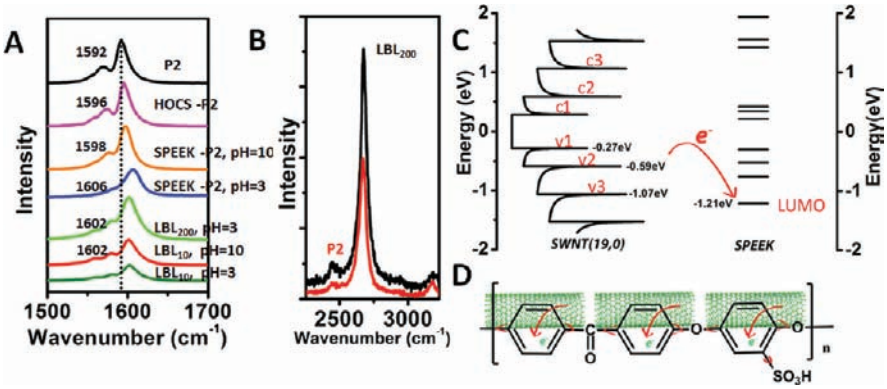

Figure 7. (A) G band in Raman spectra of as-received P2 SWNT, P2 and HOCS half−half mixtures (P2−HOCS), P2 and SPEEK 1:4 mixtures (P2−SPEEK) at pH 3 and pH 10, $[HOCS/SPEEK-P2]_{200}$ free-standing film at pH 3, and $[HOCS/SPEEK-P2]_{10}$ coatings assembled at pH 3 and pH 10. (B) G′ band of P2 SWNT and $[HOCS/SPEEK-P2]_{200}$. Excitation wavelength for all Raman spectra is 532 nm. (C) Density of states of SWNT(19,0) and energy band of SPEEK from quantum mechanical calculations. The HOMO level is at −9.28 eV for SPEEK, which is not shown in the graph. (D) Diagram of charge transfer between SPEEK and SWNT.

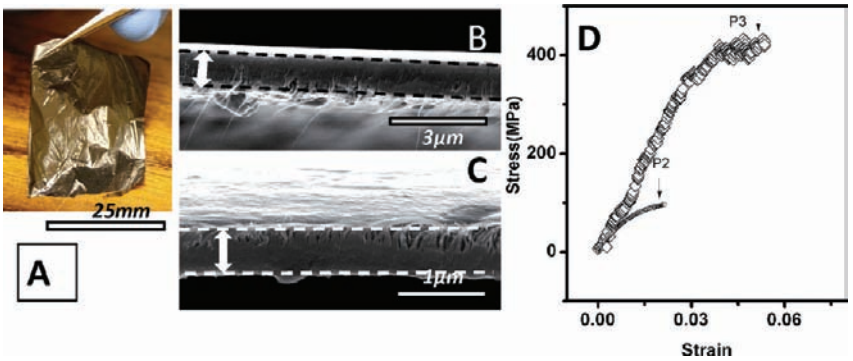

Figure 8. (A) Free-standing film of $[HOCS/SPEEK-P2]_{200}$. Cross-section images of (B) $[HOCS/SPEEK-P2]_{200}$ and (C) $[HOCS/SPEEK-P3]_{200}$. The arrows show the cross sections of films. (D) Representative stress−strain curve of $[HOCS/SPEEK-P3]_{200}$ and $[HOCS/SPEEK-P2]_{200}$.

diameter of 1.48 nm, and energy gap of S22 of 1.2 eV, representative of the SWNTs in this study. It was found that SPEEK has a much lower LUMO energy of −1.21 eV than the LUMO of PSS (−0.70 eV, Figure S7C and E), being at the same time substantially lower than the top of the valence band of SWNT (Figure 7C) located at −0.27 eV and even two other valence bands located at −0.59 and −1.07 eV. The correctness of the quantum mechanical calculation was confirmed by the excellent agreement of calculated and experimental UV spectra of SPEEK (Figure S7B). The low energy of LUMO in SPEEK, the presence of other unoccupied orbital above it, and tight wrapping of the polymer around the nanotubes (Figure 4) provide all of the necessary conditions for effective electron transfer from SWNT to SPEEK (Figure 7D). Because of the higher position of LUMO of PSS, the hole-doping by this polymer is much less effective. Also, unfavorable geometry of phenyl rings of PSS around SWNT allows less extensive π-stacking.

The charge transfer effects are also indicated by significant downshift of carbon[64] and change of oxygen photoemission peaks in the XPS spectra in the SWNT nanocomposite (Figure S8). A downshift of −2.4 eV is much larger than what was reported for hole-doping of small molecules,[29] which is usually around −0.2 eV to −0.5 eV, suggesting significant Fermi level shift due to the charge transfer. Through doping, the conductivities of semiconducting SWNT can be increased and the Schottky barrier between metallic and semiconducting SWNT can be reduced,[27] which would contribute to the improvement of overall conductivities of composite.

Mechanical Properties. Although LBL coatings from P2−SWNT have higher conductivity than those with P3−SWNT, their ultimate strength is only 90 ± 10 MPa, which is much lower than P3−SWNTmultilayers with tensile strength of 360 ± 35 MPa (Figure 8D). Stiffness and toughness followed a similar trend: 13 ± 2.4 GPa, 7.5 ± 3 kJ/m^3 as compared to 7 ± 0.4 GPa and 0.9 ± 0.3 kJ/m^3. The mechanical properties of the P2−SWNT LBL films are superior to those of bucky paper, with ultimate strength distributed from 10 to 76 MPa in ultimate strength and stiffness from 0.2 to 2 GPa.[65] More carboxylic acid groups in P3 SWNTs facilitate stronger interactions with HOCS matrix. As it was reported recently, the degree of oxidation of SWNTs can be optimized to confer the highest mechanical properties achieved so far for LBL-assembled SWNT composite.[34]

It needs to be pointed out that the mechanical strength of free-standing film can only partially reflect mechanical behavior of coatings.[66] Mechanical performance of the coatings tends to be even better on the substrate as the separation process is likely to introduce some amount of defects onto free-standing films.

Environmental Stability. Environmental stability of TCs is desirable in most of the practical applications. For example, in actual device fabrications, active layer deposition or module encapsulation usually involves moderate temperature processes,[23] and the actual

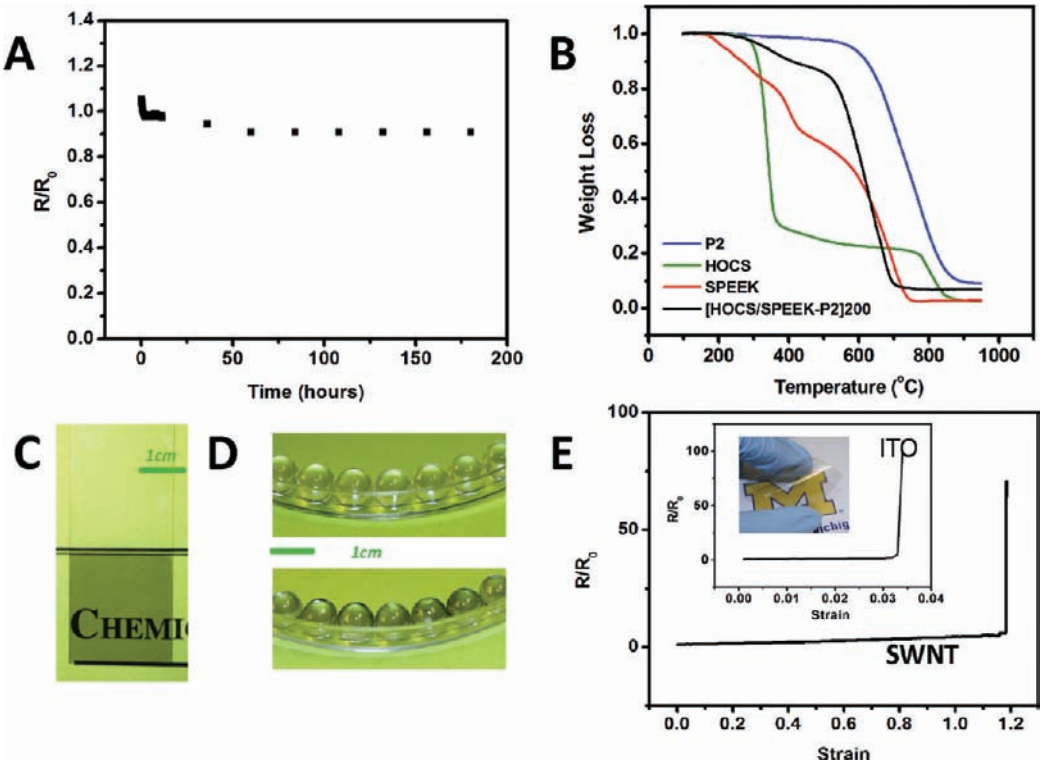

Figure 9. (A) Electrical stability of SWNT thin films at 100 °C. (B) TGA analysis of P2 SWNT, HOCS, SPEEK, and $[HOCS/SPEEK-P2]_{200}$. Flexibility of LBL method demonstrated on glass slide (C) and glass beads (D), plastic substrate (E, inset) for transparent coatings. (E) Dependence of surface resistance on stretching strain for LBL SWNT coatings and ITO on PET substrates.

device operation can also cause elevated temperatures. The electrical stability of SWNT thin films here was evaluated by exposing the film in air at 100 °C for a week, which may be one of the harshest environments in which TCs can be involved in reality (Figure 9A). Transparency of the film was not affected through this process (Figure S9). The resistance increased by 4% when the temperature was raised due to the metallic nature of the film, and then dropped quickly within 1 h as a result of thermal annealing and kept almost unchanged after 60 h. The incredible "shelf life" of the film originates from the involatility of the polymer dopant and placid nature of SWNTs. In addition, only 10% of mass loss was observed after burning in air at 500 °C, which is quite remarkable for organic coatings (Figure 9B).

The surface of coatings with few layers deposited had roughness of 3.5 nm, which was comparable to 2.4 nm of typical ITO surface or 3.1 nm for PEDOT passivated SWNT surface.[9] Additionally, these coatings could be uniformly deposited not only on planar glass slides but easily on spherical glass beads and flexible polymer substrate (Figure 9C−E). To the best of our knowledge, this is the first report to demonstrate SWNT transparent coatings on curved surfaces. LBL technique could be more competitive and advantageous over available methods when uniform, transparent, and conductive spherical surfaces are needed. The process is also amenable to scaled-up versions of TC deposition.[35]

Comparison with ITO. ITO thin films undergo catastrophic failure when the strain is over 0.03, which leads to a drastic decrease of conductivity.[11,31] On the contrary, TCs from SWNT only show a gradual increase in resistivity upon stretching; the catastrophic conduction failure only occurs when the substrate is physically pulled apart.[35] The traditional TC figure of merit (TCFM) is defined as TCFM = σ/α, where σ is electrical conductance and α is visible absorption coefficient.[67] ITO has a high TCFM, close to 4 Ω^{-1},[67] and in these terms is better than most of the reported SWNT transparent conductors. However, the traditional TCFM fails to take into account other properties highly relevant for TCs. Mechanical properties are one of the most valuable properties for the state-of-art TC; other properties could also be included in the consideration. Therefore, it would be logical to introduce a parameter of critical strain ε_c of TC into the currently used figure of merit.[35] The new TCFM can be expressed as $\prod_{TC} = \sigma\varepsilon_c/\alpha$ with the new parameter in the nominator because the larger is the critical strain, the better it is for most TC applications and in particularly for flexible electronics. ITO on polyethylene terephthalate (PET) substrate (Sigma-Aldrich) displays a sheet resistance of 60 Ω/□ at 80% (550 nm) and critical strain of 0.032 (Figure 9E),[11] which corresponds to $\prod_{TC}$ of 0.006 Ω^{-1} (Supporting Information).[72] Also, one of the best ITOs on PET reported so far was 14.19 Ω/□ at 80% (550 nm)[68] and had a $\prod_{TC}$ of 0.023 Ω^{-1}, assuming the same critical strain. For the appropriate comparison, we made SWNT LBL films on identical PET substrates. Because of the self-organizing/assembling characteristics of the LBL method, the performance of coatings is independent of substrate. The sheet resistance can be kept around 960 Ω/□ and transmittance of 86.7% at 550 nm on PET substrate using the same recipe on glass substrate (Figure 6A). The strain for catastrophic conductivity failure for them was observed at ε_c = 120% (Figure 9E).[35] $\prod_{TC}$ of the LBL assembled transparent conductor thus can be estimated to be 0.022 Ω^{-1}, which is clearly higher than that of commercial ITO, and comparable to the best ITO reported. Another interesting point to note is that experimentally elongation for catastrophic conductivity failure of thin SWNT coatings on elastic substrates is much higher than maximum mechanical

extensibility of the corresponding free-standing film of SWNT (Figure 8D). Unlike free-standing films, the coatings are stretched uniformly over both "weak" and "strong" points and can undergo, therefore, even greater extensions.

CONCLUSIONS

In this work, SPEEK has been introduced as an effective stabilizer and hole-dopant for SWNTs. It helically wraps the nanotubes, making possible effective $\pi-\pi$ stacking interactions. The alignment and effective hybridization of the unoccupied electronic levels of SPEEK and valence bands of SWNTs facilitates charge transfer comparable to or better than other dopants in effectiveness. The use of SPEEK combined with the ability of LBL technique to produce highly uniform composites with characteristically strong intermolecular interactions between the components allow for improvement of multiple parameters in SWNT-based TCs.

The cumulative hole-doping of SWNTs from SPEEK and its LBL partner, HOCS, allows one to get rid of volatile and corrosive doping agents, such as acids. Smooth and acid-free SWNT TCs with competitive transparency conductance curves were demonstrated on both planar and curved substrates. The overall performance of the fabricated TCs is better than that of commercially available ITO on PET, taking into account the critical strain of the coating material. In addition, these thin coatings demonstrate record thermal stability.

With their current performance parameters, LBL-made TCs with π-doping are suitable for many applications.[69] However, the most demanding applications, such as solar cells and LEDs, will require further reduction of the sheet resistance. Properties of SWNT TCs can be further optimized by introduction of stronger electron-withdrawing functional groups such as nitro-groups ($-NO_2$) in phenyl rings capable of $\pi-\pi$ stacking interactions with SWNTs. Calculation shows that introduction of $-NO_2$ into phenyl rings in the SPEEK unit can significantly lower the LUMO level to -4.20 eV (Figure S7D and F). In addition, selective deposition of metallic SWNT on substrate, and proper control over the alignment of SWNTs inside the composite, would be beneficial for improving the electrical conductivity of composites. It will be interesting as well to establish the detailed mechanism of doping of SWNTs by HOCS; however, it is apparently less effective than π-doping observed for SPEEK.

π-Doping with polymer can be further extended to graphene TCs. Moreover, free-standing and flexible films with high conductivity, thermal stability, and robustness obtained by LBL steps can be vital in other applications, such as neural interface[1,70] and actuators.[71]

ASSOCIATED CONTENT

Supporting Information. Complete ref 24, quantification of SWNT, tables for densities of materials, FTIR spectra for PEEK and SPEEK, mass changes upon deposition of [HOCS/SPEEK], sheet resistances/transmittance relationship for [HOCS/SPEEK−P2] and [PVA−PSS−P2], EDAX analysis, TGA results, Raman spectra for P3 SWNT, energy levels for PSS, and XPS spectra. This material is available free of charge via the Internet at http://pubs.acs.org.

AUTHOR INFORMATION

Corresponding Author
kotov@umich.edu

Present Addresses
[||]Materials Science and Engineering, University of Delaware, Newark, Delaware 19716, United States.

ACKNOWLEDGMENT

This work was primarily supported by AFOSR grants FA9550-08-1-0382, GRT00008581/RF60012388, and MURI 444286-P061716. We also acknowledge the support from NSF under grants ECS-0601345, EFRI-BSBA 0938019, CBET 0933384, and CBET 0932823 and from the National Institutes of Health under NIH 1R21CA121841-01A2. This material is based upon work partially supported by the Center for Solar and Thermal Energy Conversion, an Energy Frontier Research Center funded by the U.S. Department of Energy, Office of Science, Office of Basic Energy Sciences under Award Number #DE-SC0000957. We thank the University of Michigan's EMAL for its assistance with electron microscopy, and for the NSF grant #DMR-9871177 for funding for the NOVA analytical electron microscope used in this work.

REFERENCES

(1) Kotov, N. A.; Winter, J. O.; Clements, I. P.; Jan, E.; Timko, B. P.; Campidelli, S.; Pathak, S.; Mazzatenta, A.; Lieber, C. M.; Prato, M.; Bellamkonda, R. V.; Silva, G. A.; Kam, N. W. S.; Patolsky, F.; Ballerini, L. *Adv. Mater.* **2009**, *21*, 3970.
(2) Meyer, W. H. *Adv. Mater.* **1998**, *10*, 439.
(3) Endo, M.; Kim, Y. A.; Hayashi, T.; Nishimura, K.; Matusita, T.; Miyashita, K.; Dresselhaus, M. S. *Carbon* **2001**, *39*, 1287.
(4) Monroe, C.; Newman, J. *J. Electrochem. Soc.* **2005**, *152*, A396.
(5) Granqvist, C. G. *Sol. Energy Mater. Sol. Cells* **2007**, *91*, 1529.
(6) Ou, E. C. W.; Hu, L. B.; Raymond, G. C. R.; Soo, O. K.; Pan, J. S.; Zheng, Z.; Park, Y.; Hecht, D.; Irvin, G.; Drzaic, P.; Gruner, G. *ACS Nano* **2009**, *3*, 2258.
(7) Zhou, Y. X.; Hu, L. B.; Gruner, G. *Appl. Phys. Lett.* **2006**, 88.
(8) De, S.; Lyons, P. E.; Sorel, S.; Doherty, E. M.; King, P. J.; Blau, W. J.; Nirmalraj, P. N.; Boland, J. J.; Scardaci, V.; Joimel, J.; Coleman, J. N. *ACS Nano* **2009**, *3*, 714.
(9) Zhang, D. H.; Ryu, K.; Liu, X. L.; Polikarpov, E.; Ly, J.; Tompson, M. E.; Zhou, C. W. *Nano Lett.* **2006**, *6*, 1880.
(10) Hellstrom, S. L.; Lee, H. W.; Bao, Z. *ACS Nano* **2009**, *3*, 1423.
(11) Cairns, D. R.; Witte, R. P.; Sparacin, D. K.; Sachsman, S. M.; Paine, D. C.; Crawford, G. P.; Newton, R. R. *Appl. Phys. Lett.* **2000**, *76*, 1425.
(12) Azulai, D.; Belenkova, T.; Gilon, H.; Barkay, Z.; Markovich, G. *Nano Lett.* **2009**, *9*, 4246.
(13) Hecht, D.; Hu, L. B.; Gruner, G. *Appl. Phys. Lett.* **2006**, 89.
(14) Nomura, K.; Ohta, H.; Takagi, A.; Kamiya, T.; Hirano, M.; Hosono, H. *Nature* **2004**, *432*, 488.
(15) Myung-Gyu, K.; Myung-Su, K.; Jinsang, K.; Guo, L. J. *Adv. Mater.* **2008**, *20*, 4408.
(16) Lee, J.-Y.; Connor, S. T.; Cui, Y.; Peumans, P. *Nano Lett.* **2008**, *8*, 689.
(17) Kang, M. G.; Guo, L. J. *Adv. Mater.* **2007**, *19*, 1391.
(18) Kao, C. Y.; Lee, B.; Wielunski, L. S.; Heeney, M.; McCulloch, I.; Garfunkel, E.; Feldman, L. C.; Podzorov, V. *Adv. Funct. Mater.* **2009**, *19*, 1906.
(19) Ha, Y. H.; Nikolov, N.; Pollack, S. K.; Mastrangelo, J.; Martin, B. D.; Shashidhar, R. *Adv. Funct. Mater.* **2004**, *14*, 615.
(20) Roth, S.; Park, H. J. *Chem. Soc. Rev.* **2010**, *39*, 2477.
(21) Yamaguchi, H.; Eda, G.; Mattevi, C.; Kim, H.; Chhowalla, M. *ACS Nano* **2010**, *4*, 524.
(22) Wang, X.; Zhi, L.; Mullen, K. *Nano Lett.* **2007**, *8*, 323.
(23) Roderick, J.; Benoit, D.; Rishabh, J.; Bernard, K.; Samuel, G. *Adv. Funct. Mater.* **2008**, *18*, 2548.

(24) Bae, S.; et al. *Nat. Nanotechnol.* **2010**, *5*, 574.
(25) Geng, H. Z.; Kim, K. K.; So, K. P.; Lee, Y. S.; Chang, Y.; Lee, Y. H. *J. Am. Chem. Soc.* **2007**, *129*, 7758.
(26) Hellstrom, S. L.; Lee, H. W.; Bao, Z. N. *ACS Nano* **2009**, *3*, 1423.
(27) Kim, K. K.; Bae, J. J.; Park, H. K.; Kim, S. M.; Geng, H.-Z.; Park, K. A.; Shin, H.-J.; Yoon, S.-M.; Benayad, A.; Choi, J.-Y.; Lee, Y. H. *J. Am. Chem. Soc.* **2008**, *130*, 12757.
(28) Nirmalraj, P. N.; Lyons, P. E.; De, S.; Coleman, J. N.; Boland, J. J. *Nano Lett.* **2009**.
(29) Geng, H. Z.; Kim, K. K.; Song, C.; Xuyen, N. T.; Kim, S. M.; Park, K. A.; Lee, D. S.; An, K. H.; Lee, Y. S.; Chang, Y.; Lee, Y. J.; Choi, J. Y.; Benayad, A.; Lee, Y. H. *J. Mater. Chem.* **2008**, *18*, 1261.
(30) Siddons, G. P.; Merchin, D.; Back, J. H.; Jeong, J. K.; Shim, M. *Nano Lett.* **2004**, *4*, 927.
(31) Doherty, E. M.; De, S.; Lyons, P. E.; Shmeliov, A.; Nirmalraj, P. N.; Scardaci, V.; Joimel, J.; Blau, W. J.; Boland, J. J.; Coleman, J. N. *Carbon* **2009**, *47*, 2466.
(32) Mamedov, A. A.; Kotov, N. A.; Prato, M.; Guldi, D. M.; Wicksted, J. P.; Hirsch, A. *Nat. Mater.* **2002**, *1*, 190.
(33) Shim, B. S.; Tang, Z. Y.; Morabito, M. P.; Agarwal, A.; Hong, H. P.; Kotov, N. A. *Chem. Mater.* **2007**, *19*, 5467.
(34) Shim, B. S.; Zhu, J.; Jan, E.; Critchley, K.; Ho, S. S.; Podsiadlo, P.; Sun, K.; Kotov, N. A. *ACS Nano* **2009**, *3*, 1711.
(35) Shim, B. S.; Zhu, J.; Jan, E.; Critchley, K.; Kotov, N. A. *ACS Nano* **2010**, *4*, 3725.
(36) Reyna-Valencia, A.; Kaliaguine, S.; Bousmina, M. *J. Appl. Polym. Sci.* **2005**, *98*, 2380.
(37) Bailly, C.; Williams, D. J.; Karasz, F. E.; MacKnight, W. J. *Polymer* **1987**, 28.
(38) Devaux, J.; Delimoy, D.; Daoust, D.; Legras, R.; Mercier, J. P.; Strazielle, C.; Nield, E. *Polymer* **1985**, *26*, 1994.
(39) Louette, P.; Bodino, F.; Pireaux, J.-J. *Surf. Sci. Spectra* **2005**, *12*, 149.
(40) Wagner, C. D.; Muilenberg, G. E. *Handbook of X-ray Photoelectron Spectroscopy: A Reference Book of Standard Data for Use in X-ray Photoelectron Spectroscopy*; Perkin-Elmer Corp., Physical Electronics Division: Eden Prairie, MN, 1979.
(41) Ismail, A. F.; Othman, N. H.; Mustafa, A. *J. Membr. Sci.* **2009**, *329*, 18.
(42) Brownstein, S.; Roovers, J. *Can. J. Chem.* **1997**, *75*, 1225.
(43) Kang, Y. K.; Lee, O.-S.; Deria, P.; Kim, S. H.; Park, T.-H.; Bonnell, D. A.; Saven, J. G.; Therien, M. J. *Nano Lett.* **2009**, *9*, 1414.
(44) Tanaka, T.; Jin, H.; Miyata, Y.; Fujii, S.; Suga, H.; Naitoh, Y.; Minari, T.; Miyadera, T.; Tsukagoshi, K.; Kataura, H. *Nano Lett.* **2009**, *9*, 1497.
(45) Green, A. A.; Hersam, M. C. *Nano Lett.* **2008**, *8*, 1417.
(46) Arnold, M. S.; Green, A. A.; Hulvat, J. F.; Stupp, S. I.; Hersam, M. C. *Nat. Nano* **2006**, *1*, 60.
(47) Weisman, R. B.; Bachilo, S. M. *Nano Lett.* **2003**, *3*, 1235.
(48) Chen, J.; Liu, H.; Weimer, W. A.; Halls, M. D.; Waldeck, D. H.; Walker, G. C. *J. Am. Chem. Soc.* **2002**, *124*, 9034.
(49) Naito, M.; Nobusawa, K.; Onouchi, H.; Nakamura, M.; Yasui, K.-i.; Ikeda, A.; Fujiki, M. *J. Am. Chem. Soc.* **2008**, *130*, 16697.
(50) Gigliotti, B.; Sakizzie, B.; Bethune, D. S.; Shelby, R. M.; Cha, J. N. *Nano Lett.* **2006**, *6*, 159.
(51) Wu, G.-M.; Schultz, J. M. *Angew. Makromol. Chem.* **1998**, *257*, 53.
(52) McAllister, M. J.; Li, J.-L.; Adamson, D. H.; Schniepp, H. C.; Abdala, A. A.; Liu, J.; Herrera-Alonso, M.; Milius, D. L.; Car, R.; Prud'homme, R. K.; Aksay, I. A. *Chem. Mater.* **2007**, *19*, 4396.
(53) Whitby, R. L. D.; Fukuda, T.; Maekawa, T.; James, S. L.; Mikhalovsky, S. V. *Carbon* **2008**, *46*, 949.
(54) Kotov, N. A. *Nanostruct. Mater.* **1999**, *12*, 789.
(55) Brothers, E. N.; Izmaylov, A. F.; Scuseria, G. E.; Kudin, K. N. *J. Phys. Chem. C* **2008**, *112*, 1396.
(56) Brothers, E. N.; Scuseria, G. E.; Kudin, K. N. *J. Phys. Chem. B* **2006**, *110*, 12860.
(57) Han, J. T.; Kim, J. S.; Jeong, H. D.; Jeong, H. J.; Jeong, S. Y.; Lee, G.-W. *ACS Nano* **2010**, *4*, 4551.
(58) Podsiadlo, P.; Sui, L.; Elkasabi, Y.; Burgardt, P.; Lee, J.; Miryala, A.; Kusumaatmaja, W.; Carman, M. R.; Shtein, M.; Kieffer, J.; Lahann, J.; Kotov, N. A. *Langmuir* **2007**, *23*, 7901.
(59) Blighe, F. M.; Hernandez, Y. R.; Blau, W. J.; Coleman, J. N. *Adv. Mater.* **2007**, *19*, 4443.
(60) Wang, G.-F.; Tao, X.-M.; Wang, R.-X. *Nanotechnology* **2008**, *19*, 145201.
(61) Kim, K. K.; Park, J. S.; Kim, S. J.; Geng, H. Z.; An, K. H.; Yang, C.-M.; Sato, K.; Saito, R.; Lee, Y. H. *Phys. Rev. B* **2007**, *76*, 205426.
(62) Duclaux, L. *Carbon* **2002**, *40*, 1751.
(63) Moonoosawmy, K. R.; Kruse, P. *J. Am. Chem. Soc.* **2010**, *132*, 1572.
(64) Graupner, R.; Abraham, J.; Vencelova, A.; Seyller, T.; Hennrich, F.; Kappes, M. M.; Hirsch, A.; Ley, L. *Phys. Chem. Chem. Phys.* **2003**, *5*, 5472.
(65) Xu, G. H.; Zhang, Q.; Zhou, W. P.; Huang, J. Q.; Wei, F. *Appl. Phys. A: Mater. Sci. Process.* **2008**, *92*, 531.
(66) Chen, J.; Bull, S. J. *J. Phys. D: Appl. Phys.* **2007**, *40*, 5401.
(67) Gordon, R. G. *MRS Bull.* **2000**, *25*, 52.
(68) Sandoval-Paz, M. G.; Ramírez-Bon, R. *Thin Solid Films* **2009**, *517*, 2596.
(69) Kaempgen, M.; Duesberg, G. S.; Roth, S. *Appl. Surf. Sci.* **2005**, *252*, 425.
(70) Jan, E.; Kotov, N. A. *Nano Lett.* **2007**, *7*, 1123.
(71) Shim, B. S.; Chen, W.; Doty, C.; Xu, C. L.; Kotov, N. A. *Nano Lett.* **2008**, *8*, 4151.
(72) ITO on PET substrate (Sigma-Aldrich) displays a sheet resistance of 60 Ω/□ at 80% (550 nm) and critical strain of 0.032 (Figure 9E). The figure of merit, $\prod_{TC}$, can thus be calculated to be 0.007. In our previous publication, we estimated $\prod_{TC}$ of ITO was 0.07 Ω^{-1} by using the best property of ITO reported on glass: 6 Ω/□ at 90%[67] and critical strain of 1.7% [see Chen, Z.; et al. *Thin Solid Films* **2001**, *394*, 201−205]. When drafting this Article, we realized that the performance of ITO on plastic substrate, such as PET, is much worse due to the low processing temperature required for polymer substrate. Thus, in this Article, we quoted the best results of ITO on PET substrate and tested the commercially available ITO in our lab. We believe these data can more accurately reflect the real performance of ITO on PET.